Model Predictive Direct Speed Control with Finite Control Set of PMSM Drive Systems

Matthias Preindl and Silverio Bolognani, *Member, IEEE*

***Abstract*—Servo drives and drives for position control require a high dynamic on speed control. In this paper, model predictive direct speed control (MP-DSC) is proposed, which overcomes limitations of cascaded linear controllers. The novel concept predicts the future current and speed states in discrete steps and it selects plant inputs which depends mainly on the predicted speed error. Secondary control objectives, such as maximum torque per ampere tracking are included. MP-DSC uses the finite control set approach which makes it suitable for online predictions with a prediction horizon of a few sample periods. The concept has been developed by simulation and evaluated on an experimental test bench. The overall control behavior is evaluated applying reference and disturbance steps to the system, where MP-DSC shows promising results. A solution for disturbance (e.g., load toque) rejection is proposed, and the effectiveness to avoid control offsets is shown. Furthermore, the dynamic performance and the steady-state behavior of MP-DSC is evaluated and discussed.**

***Index Terms*—Drive Systems, direct speed control (DSC), model predictive control (MPC), permanent magnet synchronous machine (PMSM).**

NOMENCLATURE

$R \in \mathbb{R}_+$	Stator resistance.
$L_d, L_q \in \mathbb{R}_+$	Stator inductance (d, q axis, respectively).
$\lambda \in \mathbb{R}_+$	PM flux linkage.
$B \in \mathbb{R}_+$	Friction coefficient.
$J \in \mathbb{R}_+$	Inertia coefficient.
$u_d, u_q \in \mathbb{R}$	Stator voltage (d, q axis, respectively).
$i_d, i_q \in \mathbb{R}$	Stator current (d, q axis, respectively).
$I_r \in \mathbb{R}_+$	Rated stator current.
$N_u \in \mathbb{N}_+$	Number of inverter switching states.
$\theta \in \mathbb{R}$	Electrical rotor angle.
$\omega \in \mathbb{R}$	Electrical rotor speed.
$T_e \in \mathbb{R}$	Electrical torque.
$T_l \in \mathbb{R}$	Load torque.
$t \in \mathbb{R}_+$	Time.
$T_s \in \mathbb{R}_+$	Sampling period.
$k \in \mathbb{N}_+$	Sample.
$N \in \mathbb{N}_+$	Prediction horizon.
$T_x \in \mathbb{R}_+$	Execution time.
$\cdot^*$	Reference value.
$\hat{\cdot}$	Estimated value.
$x \in \mathbb{R}^n, n \in \mathbb{N}_+$	Plant states.
$u \in \mathbb{R}^m, m \in \mathbb{N}_+$	Controlled plant inputs.
$w \in \mathbb{R}^p, p \in \mathbb{N}_+$	Disturbance input.
$v \in \mathbb{R}^q, q \in \mathbb{N}_+$	Compensation input.
$y \in \mathbb{R}^r, r \in \mathbb{N}_+$	Measurements.
$\mathbf{A} \in \mathbb{R}^{n \times n}$	State parameter matrix.
$\mathbf{B} \in \mathbb{R}^{n \times m}$	Input parameter matrix.
$\mathbf{E} \in \mathbb{R}^{n \times p}$	Disturbance parameter matrix.
$\mathbf{L} \in \mathbb{R}^{n \times q}$	Compensation parameter matrix.
$\mathbf{C} \in \mathbb{R}^{r \times n}$	Measurement parameter matrix.
$\cdot_e$	Referred to the electric system.
$\cdot_m$	Referred to the mechanic system.

Manuscript received February 20, 2012; revised April 17, 2012; accepted May 26, 2012. Date of current version September 27, 2012. Recommended for publication by Associate Editor K. M. Ralph.

The authors are with the Department of Industrial Engineering, University of Padova, 35131 Padova, Italy (e-mail: matthias.preindl@gmail.com; bolognani@die.unipd.it).

Color versions of one or more of the figures in this paper are available online at http://ieeexplore.ieee.org.

Digital Object Identifier 10.1109/TPEL.2012.2204277

I. INTRODUCTION

SERVO drives and drives for position control require high dynamics on speed control. Cascade linear controllers have a limited bandwidth in order to avoid large overshoots and ringing and due to their cascaded structure, where the different loops are decoupled in bandwidth. These structures limit the dynamics above all in high power applications, where the switching frequency is low. In this cases, the bandwidth of the current controllers is already low resulting in a fairly modest speed (or position) control dynamic.

In order to increase dynamics, different predictive control approaches have been investigated in past and they are shown in the literature [1]. Examples are deadbeat [2], hysteresis based [3], trajectory-based control [4] or combinations of the concepts like sliding mode [5] and direct torque control [6]. However, most concepts which have been presented in the literature focus either on current or torque/flux control, which still requires a cascade speed loop. These limitations are overcome with direct speed control approaches, e.g., [7]–[9].

In contrast to the cited concepts, model predictive control (MPC), e.g., [10]–[14], can take into account constraints and nonlinearities of multiple input and multiple output plants and handle them in an unified manner. MPC can be divided in continuous control set and finite control set methods. The latter one needs in contrast to the first one no modulator [like space vector modulation (SVM) or pulse-width modulation (PWM)] and it is suitable for online optimization. On the other hand, it has a variable switching frequency.

In this paper, the (finite control set) model predictive direct speed control (MP-DSC) is proposed, which overcomes limitations by cascaded loops resulting in high-speed control dynamics (see Fig. 1). The controller is based on the finite control set (FCS) MPC approach, i.e., the switching states of the power electronic converter are taken into account and a modulation scheme is avoided. A novel cost function is proposed

in this paper for direct speed control. It is subdivided in a *tracking component*, an *attraction region*, and *limitations*. The tracking component is used to track the reference value. Plant limits are included in the model, and inputs which would lead to a violation of those limits are avoided. Besides speed control, secondary control goals, e.g., concerning efficiency, can be included in using control formulation. The attraction region becomes important when the tracking component is small, i.e., at steady state. Moreover, a new way for disturbance and noise rejection is proposed. It improves above all the steady-state performance. Control offsets and switching due to measurement noise are avoided. Moreover, a switching state graph, which is known from model predictive direct current control (MP-DCC) [15], [16], has been introduced for keeping the switching frequency of MP-DSC low. Another benefit of the graph is the reduction of the computation time.

This paper is organized as follows. The plant is analyzed and shown in Section II, where also the main control goals are defined. In Section III, MP-DSC is synthesized and the required techniques are shown: past input compensation, state prediction, disturbance handling, state limitations, and the plant input selection via cost function. Furthermore, MP-DSC is tested and the results are shown in Section IV. The overall control behavior is evaluated such as the control offset suppression, the dynamic and steady-state behavior.

II. Analysis

A. Plant

The continuous time, permanent magnet synchronous machine (PMSM) model, which works with isotropic (or surface) and anisotropic (or interior) PMSM, is in the dq reference frame

$$\begin{aligned} \dot{i_d} &= -\frac{R}{L_d} i_d + \frac{L_q}{L_d}\omega i_q + \frac{1}{L_d} u_d \\ \dot{i_q} &= -\frac{R}{L_q} i_q - \frac{L_d}{L_q}\omega i_d + \frac{1}{L_q} u_q - \frac{\lambda}{L_q}\omega \\ T_e &= \frac{3}{2} p(\lambda i_q + (L_d - L_q) i_d i_q) \\ \dot{\omega} &= -\frac{B}{J}\omega + \frac{p}{J} T_e - \frac{p}{J} T_l. \end{aligned} \tag{1}$$

The model can be rewritten in discrete time. The electrical state-space model is

$$\begin{aligned} x_e(k+1) &= \mathbf{A}_e x_e(k) + \mathbf{B}_e u_e(k) + \mathbf{E}_e \\ y_e(k) &= \mathbf{C}_e x_e(k) \end{aligned} \tag{2}$$

where $x_e = y_e = [i_d, i_q]^T$, $u_e = [u_d, u_q]^T$, and

$$\mathbf{A}_e = \begin{bmatrix} 1 - \dfrac{RT_s}{L_d} & \dfrac{L_q T_s}{L_d}\omega \\ -\dfrac{L_d T_s}{L_q}\omega & 1 - \dfrac{RT_s}{L_q} \end{bmatrix} \qquad \mathbf{B}_e = \begin{bmatrix} \dfrac{T_s}{L_d} & 0 \\ 0 & \dfrac{T_s}{L_q} \end{bmatrix}$$

$$\mathbf{E}_e = \begin{bmatrix} 0 \\ -\dfrac{\lambda T_s}{L_q}\omega \end{bmatrix} \qquad \mathbf{C}_e = \begin{bmatrix} 1 & 0 \\ 0 & 1 \end{bmatrix}.$$

The matrices $\mathbf{A}_e$ and $\mathbf{E}_e$ depend on ω, which requires their update during the execution of MP-DSC. The electrical torque can be calculated depending on $x_e(k)$

$$T_e(k) = \frac{3}{2} p\,(\lambda i_q(k) + (L_d - L_q) i_d(k) i_q(k)) \tag{3}$$

The discrete mechanical state-space model is

$$\begin{aligned} x_m(k+1) &= \mathbf{A}_m x_m(k) + \mathbf{B}_m u_m(k) + \mathbf{E}_m w_m(k) \\ y_m(k) &= \mathbf{C}_m x_m(k) \end{aligned} \tag{4}$$

where $x_m = \omega$, $u_m = T_e$, $w_m = T_l$, and

$$\mathbf{A}_m = 1 - \frac{BT_s}{J} \qquad \mathbf{B}_m = \frac{pT_s}{J}$$

$$\mathbf{E}_m = -\frac{pT_s}{J} \qquad \mathbf{C}_m = 1.$$

A voltage source inverter (VSI) can apply a finite set of voltages U_e to the motor, i.e., $u_e(k) \in U_e \subset \mathbb{R}^{m_e}$ (further called input). Thus, the possible electrical and mechanical states are $x_e(k) \in X_e \subset \mathbb{R}^{n_e}$ and $x_m(k) \in X_m \subset \mathbb{R}^{n_m}$, respectively. Thus, future values of the states can be computed knowing the previous inputs and states of the system.

Observation: $u_e(k)$ is the plant input, which is generated by the VSI. $u_m(k)$ is a consequence of the state $x_e(k)$. Thus, the input $u_e(k)$ leads to $x_e(k+1)$ and $x_m(k+2)$ taking into account the previous values, but $x_m(k+1)$ is independent of $u_e(k)$ and depends on $u_e(k-1)$. For evaluation of the convenience of an input, the values must be used which are dependent on the same input.

Moreover, the execution of a control algorithm takes a certain time $T_x > 0$. Thus, a practical implementation relies on measurements which are obtained previously, e.g., $y_e(k-1)$ and $y_m(k-1)$. For high performance control, the state variation between measurement and actuation instant should be compensated.

B. Control

The minimum requirements on a controller of a discrete time system is, besides practical asymptotic stability [17], the tracking of a reference signal, i.e., $\lim_{t\to+\infty} \|x - x^*\| < \epsilon$, where $\epsilon \in \mathbb{R}$ is small. In the case of a speed controller, i.e., MP-DSC, the goal is $\lim_{t\to+\infty} \|x_m - x_m^*\| < \epsilon$.

Moreover, a plant has limits for the states and inputs. MPC takes implicitly input limits into account but the states must be limited to their rated values $x(k) \leq x_r$, where $x_r \in \mathbb{R}^n$. In this paper, the x_m is assumed to be limited externally by limiting the reference value. On the other hand, the electrical states, i.e., the current amplitude must be limited to the maximum admissible value, i.e., $\|x_e\| \leq I_r$.

Additional demands on the control algorithm may arise. For example, high current quality leads to a small toque ripple, or the machine should work close to the maximum torque per ampere (MTPA) trajectory in order to obtain a high steady state, i.e.,

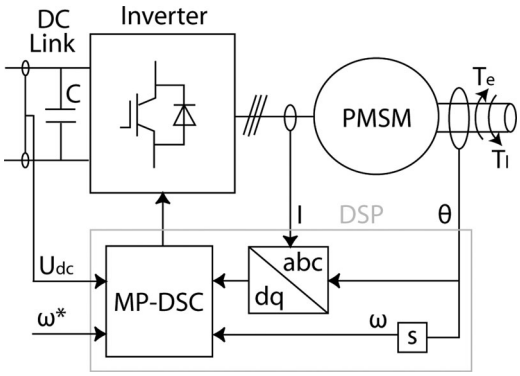

Fig. 1. PMSM-VSI drive system.

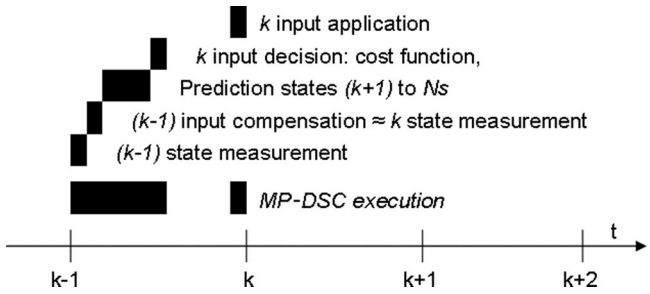

Fig. 2. Execution of the MP-DSC algorithm.

equilibrium condition efficiency. If over-speed capabilities are desired, the controller must work off the MTPA trajectory in order to weaken the stator flux.

III. Synthesis

In this section, the execution of the MP-DSC algorithm is shown. The operation can be divided in four main parts: measurement, prediction, input selection, and actuation. First, the necessary states are measured in period $(k-1)$ and concepts for compensating the delays and rejecting the disturbances are executed. Then, future plant states are computed for the periods $(k+1),\ldots,N$. The results are evaluated with a cost function and the input with the lowest cost will be applied in period k. The MP-DSC execution is shown in Fig. 2.

A. Measurement

1) Delay Compensation: The measurements from the previous sampling instant are assumed to be available for control, i.e., the available measurements are: $y_e(k-1)$ and $y_m(k-1)$. The states changes due to the system itself $x(k-1)$, the inputs $u(k-1)$, and the disturbances $w(k-1)$. Compensation is necessary in order to apply the input $u_e(k)$ to the state for which it has been computed for. Thus, the model (2) and (4) is used to compute the states $x(k)$ using $y(k-1)$, $u(k-1)$, and, if known, $w(k-1)$.

Moreover, $x_m(k+1)$ depends on $u_m(k)$ and $u_e(k-1)$. Therefore, $x_m(k+1)$ is independent of future inputs and can be calculated.

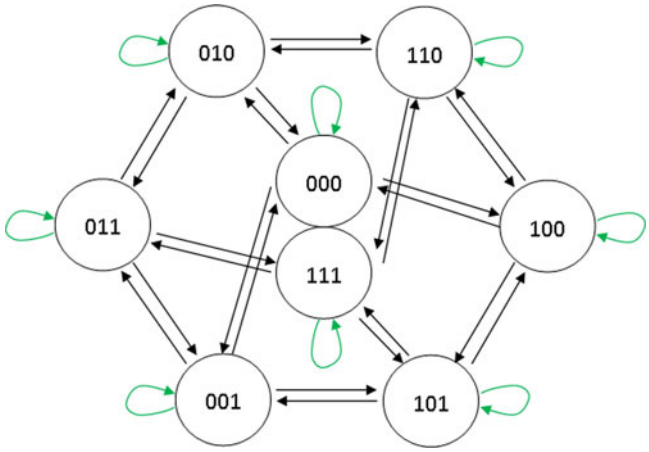

Fig. 3. Switch-state graph with possible changes.

2) Disturbance Rejection: The disturbance input $w(k)$ is generally unknown and leads to prediction errors if it is not compensated. In MP-DSC, the most important disturbance is the mechanical or further called load torque, whose measurement should be avoided due to cost and reliability reasons. A possible approach is to estimate the load torque [18]. On the other hand, estimation errors and offsets can also be the consequence of parameter uncertainties, modeling errors, etc. Thus, a more general compensation of prediction offsets is desired.

A possible approach is to see the prediction as estimation process, which is corrected with the measurements. The method, which is shown in this section is based on the state-observer principle [19]. The observer

$$\begin{aligned}\hat{x}(k+1) &= \mathbf{A}\hat{x}(k)+\mathbf{B}u(k)+\mathbf{L}_P v_P(k)+\mathbf{L}_I v_I(k)\\ v_I(k+1) &= v_I(k)+T_s v_P(k)\\ \hat{y}(k) &= \mathbf{C}\hat{x}(k)\end{aligned} \tag{5}$$

where $v_P(k)=(y(k)-\hat{y}(k))=\mathbf{C}(x(k)-\hat{x}(k))$ and $\mathbf{L}_P$, $\mathbf{L}_I\in\mathbb{R}^{n\times q}$, is placed in parallel to the plant

$$\begin{aligned}x(k+1) &= \mathbf{A}x(k)+\mathbf{B}u(k)+\mathbf{E}w(k)\\ y(k) &= \mathbf{C}x(k)\end{aligned} \tag{6}$$

which is used for both the electrical and the mechanical systems. Using this approach, the effect of disturbances are compensated by integration. The dynamics of the compensation can be adjusted acting on the gains $\mathbf{L}_P$ and $\mathbf{L}_Q$.

Additionally, this approach contributes to noise rejection. Measurements noise can have a bad influence on the steady-state performance. In this case, the control error is small and the noise can lead to undesired switching actuation resulting in a worse current, i.e., torque, quality. Using the measurement observer, this phenomena is avoided.

B. Prediction

1) Input Preselection: The possible inputs $u_e(k)\in U_e$ which can be applied after a given input $u_e(k-1)$ are additionally limited by a switch state graph similar to [15] (see Fig. 3).

Such a graph has several benefits. First, the switching frequency is limited since only one switch state change is permitted per sampling period. The application of two opposite voltage vectors is avoided leading to a lower current ripple. Moreover, the number of predictions, which must be computed, is limited, e.g., $(N_u/2)^N$ instead of $(N_u)^N$ for a two-level inverter.

2) State Prediction: The states $x_e(k+1)$ and $x_m(k+2)$ depend on their previous values and $u_e(k)$. Since $u_e(k) \in U_e$ is a finite number $N_i \in \mathbb{N}_0$ of u_d and u_q combinations, the possible future states are a finite set and can be computed. If the prediction horizon is $N > 1$, the future states are used to calculate the states of the prediction period $j \in \mathbb{N}_+$, i.e., $x_e(k+j)$ and $x_m(k+1+j)$.

The prediction process can be seen as recursive function, which calls itself until the prediction period is equal to the prediction horizon. The number of predictions increases exponentially with N. Thus, the choice of N is critical for real-time implementations. Usually the prediction horizon cannot be more than a few samples.

C. Input Selection

The possible inputs $u(k)$ are evaluated using an optimality criterion. Optimality can be obtained only with respect to a mathematical criteria, i.e., the cost function, and the input with the best performance, i.e., with the minimum cost, is chosen for application. The recursive prediction algorithm calculates the path with the minimum cost ahead. The cost of the actual prediction period is added to the path with the lowest cost ahead. Thus, the path with the globally lowest cost is constructed. Then, the first input of the optimal sequence is applied to the plant.

1) Tracking: The main goal of MP-DSC is the minimization of the speed error. Thus, the cost for a speed error is

$$c_T(k) = \left(\omega(k) - \omega^*(k)\right)^2 \tag{7}$$

which is one of the main components of the cost function.

2) Attraction Region: If the reference tracking error is large (transient behavior), the main focus of the controller should be the reduction of $c_T(k)$. However, when the tracking error is small (approximately, i.e., semisteady-state behavior), secondary control goals can be focused. This behavior is achieved by adding the secondary control goals to the cost function weighting them less than the tracking component. Thus, the system states are "attracted" to the secondary control goals in semisteady-state conditions. Otherwise, the so-called attraction region will be ignored.

The attraction region is designed to have influence on the input selection when c_T is small. A main steady-state concern is the system efficiency. Low absolute currents are desired in order to avoid large losses, i.e., to obtain a high electrical efficiency. For this reason, the MTPA criteria [20], is used

$$c_{A1}(k) = \left(i_d + \frac{L_d - L_q}{\lambda}\left(i_d^2 - i_q^2\right)\right)^2 \tag{8}$$

which defines the trajectory in the i_d, i_q space.

Above the rated speed, the machine must work off the MTPA trajectory. Thus, another attraction region close to the voltage limit is defined

$$c_{A2}(k) = \left(\sqrt{\left(\frac{L_q}{L_d} i_q\right)^2 + \left(i_d + \frac{\psi}{L_d}\right)^2} - \frac{\zeta U_c}{\sqrt{3}\omega L_d}\right)^2 \tag{9}$$

where $\zeta \in [0,1] \subset \mathbb{R}_+$ is a safety factor.

c_{A1} and c_{A2} are generally nonzero and influence each other. Thus, it is necessary to choose, which attraction region is active and ignore the other. A convenient choice is $c_A = c_{A2}$, if:

1) the state is located on the left side of the MTPA trajectory;
2) $c_{A2}(k) < c_{A1}(k)$.

otherwise $c_A = c_{A1}$.

In [21] and [22], the design of the attraction region is discussed and evaluated in detail.

3) Control Limitations: Control limitations need to be taken into account when designing the controller. The proposed MP-DSC uses a concept which is very close to the concept of soft constraints. The controller may violate limits, but any violation is penalized heavily in the cost function. Thus, if a violation happens it lasts only for a short time and generally violation of limits in steady-state conditions is avoided. In practice, the constraints are design as piecewise quadratic functions, which are zero when the limit is not violated and increases quadratically if it is.

A power converter and electrical machine have a maximum absolute current. The plant current must be limited to this value

$$c_{L1}(k) = \begin{cases} \left(I_r - \sqrt{i_d^2 + i_q^2}\right)^2 \Big| I_r - \sqrt{i_d^2 + i_q^2} < 0 \\ 0. \end{cases} \tag{10}$$

Moreover, (8) has two solutions and it is axis symmetric, but only one solution corresponds to the MTPA trajectory. In order to avoid convergence to the wrong solution, the state should remain on the correct side of the symmetry axis

$$c_{L2}(k) = \begin{cases} \left(2\frac{L_d - L_q}{\psi} i_d + 1\right)^2 \Big| 2\frac{L_d - L_q}{\psi} i_d + 1 < 0 \\ 0. \end{cases} \tag{11}$$

For operation at high speeds, the voltage limit must be taken into account

$$\xi = \sqrt{\left(L_q i_q\right)^2 + \left(L_d i_d + \psi\right)^2} - \frac{\zeta U_c}{\sqrt{3}\,|\omega|}$$

$$c_{L3}(k) = \begin{cases} \xi^2 \,|\xi < 0 \\ 0. \end{cases} \tag{12}$$

The cost c_L due to the limitations is $c_L = c_{L1} + c_{L2} + c_{L3}$.

TABLE I
PLANT DATA

Control	
Sampling time T_s	$100\mu s$
Prediction horizon N_s	3
Theoretic peak switching freq. f_{swp}	$1.66kHz$
λ_T	1
λ_A	10^{-3}
λ_L	10^4
Encoder (number of pulses)	$2048ppr$
DSP (TMS320F240) freq.	$20MHz$
Max possible N_s (computational limit)	4
Converter	
Type	2-level VSI
DC-link voltage U_{dc}	$200V$
Rated current I_r	$10A$
Interlock time T_i	$1\mu s$
Electrical Machine	
Type	IPMSM
Rated machine speed ω_r	$3000rpm$
ω_r without field-weakening	$1200rpm$
Rated torque T_r	$7.8Nm$
Inductance (d axis) L_d	$12mH$
Inductance (q axis) L_q	$20mH$
Stator resistance R	$636m\Omega$
PM rotor flux ψ	$88mWb$
Pole pairs p	5
Friction constant B	$1.7 \cdot 10^{-3} kgm/s^2$
Inertia constant J	$1.0 \cdot 10^{-3} kgm^2$

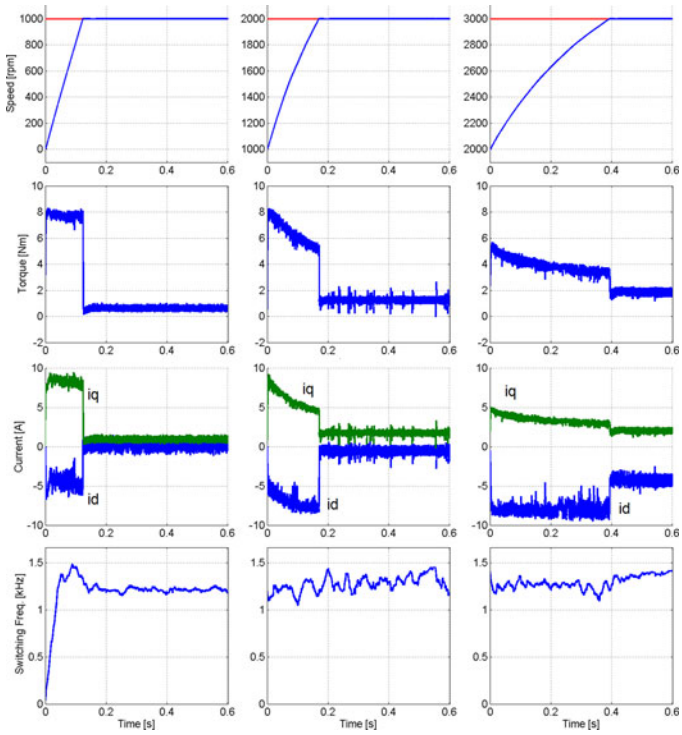

Fig. 4. Simulation result: speed reference steps; from top: reference and measured speed, and electrical torque.

In [21] and [22], the design of the limitations is discussed and evaluated in detail.

4) Cost Function: The cost function is defined with

$$C(k) = \sum_{i=0}^{N} \begin{pmatrix} \lambda_T c_T(k+i) + \\ +\lambda_A c_A(k+i) + \\ +\lambda_L c_L(k+i) \end{pmatrix} \tag{13}$$

where λ_T, λ_A, and λ_L are weighting coefficients, which define the importance of a goal with respect to the others.

IV. EVALUATION

The concept has been applied to a PMSM-VSI drive system in simulation and on an experimental test bench. The test system characteristics are shown in Table I. The MP-DSC performance has been evaluated and the results are shown in this section.

A. Speed Reference Step

In order to evaluate the control behavior, different speed reference steps have been applied to the system. Above the rated speed, a negative d current must be injected to weaken the stator flux. Otherwise, the stator voltage tends to raise above the rated voltage of the drive and the speed cannot be increased anymore. The drawback is the reduction of the available torque since the current is partially used for flux weakening. Moreover, the field weakening region can be further divided. Above a certain velocity, a negative d current is also necessary at steady state for meeting the voltage limit.

The first speed reference step is 0–1000 r/min. 1000 r/min is below rated speed and no field weakening is necessary. The electric states stay on the MTPA trajectory. The second speed reference step is 1000 to 2000 r/min. At 2000 r/min, peak torque cannot be obtained anymore since it would lead to a violation of the voltage limit. However, no d current injection is required for operation at 2000 r/min without load torque. Thus, the step can be seen as step from the standard operation region to the field weakening region. The third step is from 2000 to 3000 r/min. At 3000 r/min, d current must be injected also without producing significant torque in order to fulfil the voltage limit.

The simulation results are shown in Fig. 4 and the experimental results are shown in Fig. 5. In this figure, the reference and measured speed are shown. Moreover, the electrical torque, the dq currents, and the switching frequency are shown.

When the steps are applied, the tracking component is dominant. Thus, high torque is applied until the speed error becomes small. When this happens, the attraction region becomes important. The lowest admissible current should be applied which permits to maintain the speed. Electrical torque is still necessary to compensate the mechanical losses at steady state even if no load torque is applied. The states remain close to the MTPA

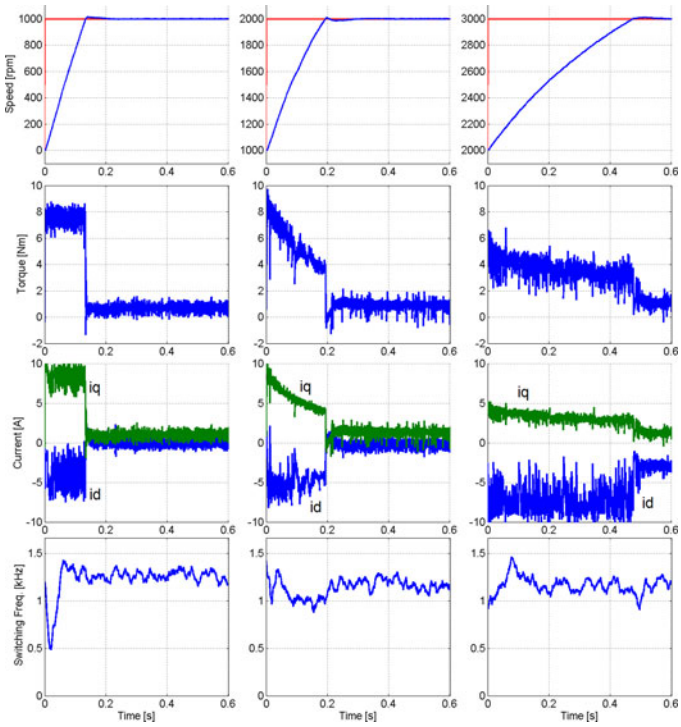

Fig. 5. Experimental result: speed reference steps; from top: reference and measured speed, and electrical torque.

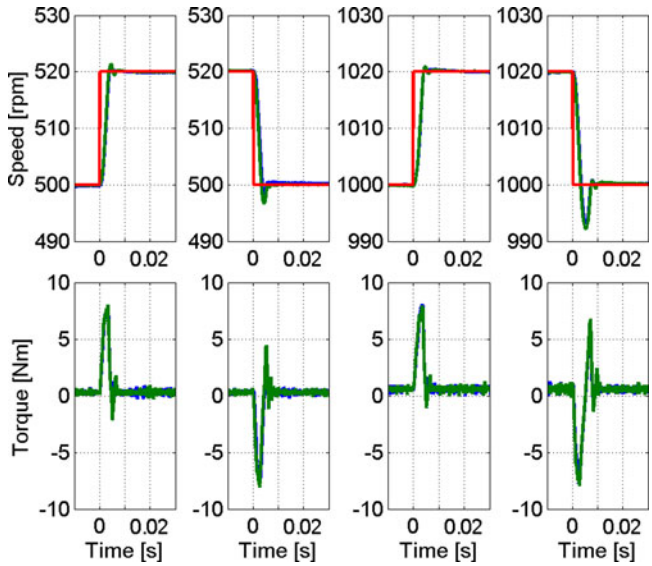

Fig. 6. Simulation result: two (blue and green) speed reference steps without torque saturation (20 rpm $= 0.6\%$); from top: reference and measured speed, and electrical torque.

trajectory at low speed and close to the voltage limit at high speed.

The switching frequency of FCS-MPC concepts is variable but above all medium and high power converters have a maximum, i.e., rated switching frequency due to thermal constraints. The switching frequency is shown in both Figs. 4 and 5 for completeness. Its peak value is limited to 1.666 kHz due to the state graph, but it will stay below on average.

B. Dynamics

The speed control performance of the system is evaluated in this section. Small speed reference steps have been applied to the system. The steps are scaled in order to avoid saturation of the system, in first place the limitation of the torque, i.e., the currents.

Since the system is nonlinear, it is difficult to find analytical performance indexes like the high frequency cutoff (which corresponds to the bandwidth due to the low-pass behavior). However, a Gaussian response $H(\omega) = e^{-\frac{\omega^2}{\sigma^2}}$ can be assumed in order to give an idea about performance. Thus, the further called *practical bandwidth* f_{bw} of the corresponding system can be approximated knowing the 10%–90% rise time t_r using [23]

$$f_{\mathrm{bw}} = \frac{0.34}{t_r}. \tag{14}$$

The step responses have been studied and they are shown in Figs. 6 and 7. The average raise times are about $t_r = 3$ ms and $t_r = 5$ ms, and the corresponding practical bandwidths are $f_{\mathrm{bw}} = 113$ and 68 Hz in simulation and experimentation, respectively. The experimental result is slightly worse than the simulated one. This is due to the encoder, which produces a speed measurement with an overlaid discrete noise. In simulation, the effect has not been taken into account.

C. Load Torque

The main disturbance, i.e., the load torque, tends to lead to prediction errors. Generally, it cannot be compensated since a measure must be avoided due to cost and reliability considerations. A potential error influences the evaluation using the cost function and results in a speed offset. Of course, such an offset should be avoided. Improvement comes along using the compensation, which is shown in Section III-A2. The disturbance is compensated forcing the error between predicted and measured speed to zero. This implies that the offset in speed regulation is compensated.

The concept is evaluated in simulation in Fig. 8 and experimentally in Fig. 9. A load torque step $T_l = 6$ N·m (about 80%) is applied at $n = 500$ r/min. The resulting speed variation is 110 r/min (about 3.5%) before it gets compensated. In the figures, the reference and measured speed, the electrical torque, the dq currents, and the switching frequency are shown.

D. Torque Quality

MP-DSC does not control explicitly the currents to a sinusoidal value. Thus, steady-state tests have been performed in order to show the current, i.e., torque quality. The load torque $T_l = 6$ N·m is applied at $n = 500$ r/min. The results are shown in Figs. 10 and 11.

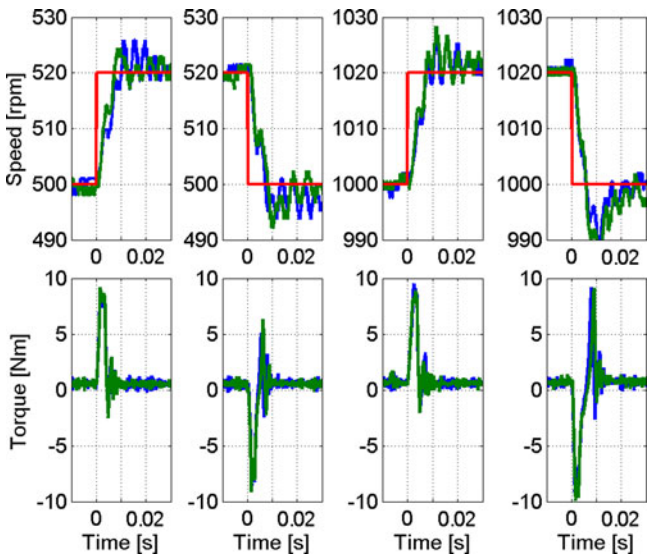

Fig. 7. Experimental result: two (blue and green) speed reference steps without torque saturation (20 rpm = 0.6%); from top: reference and measured speed (0.2% encoder discretization noise), and electrical torque.

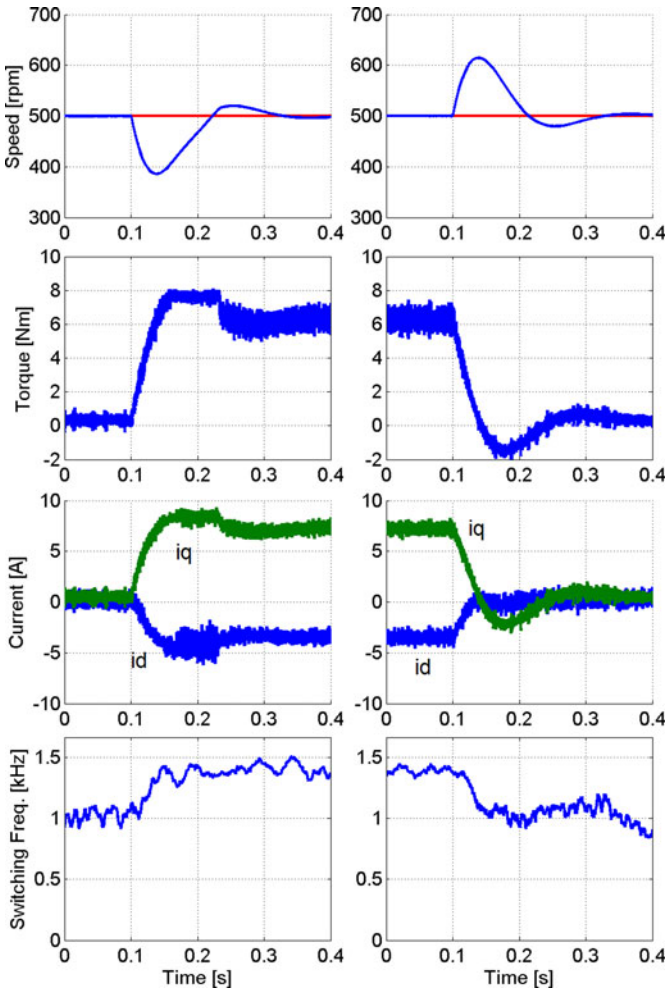

Fig. 8. Simulation result: load torque step; from top: reference and measured speed, electrical torque, *dq* currents, and switching frequency.

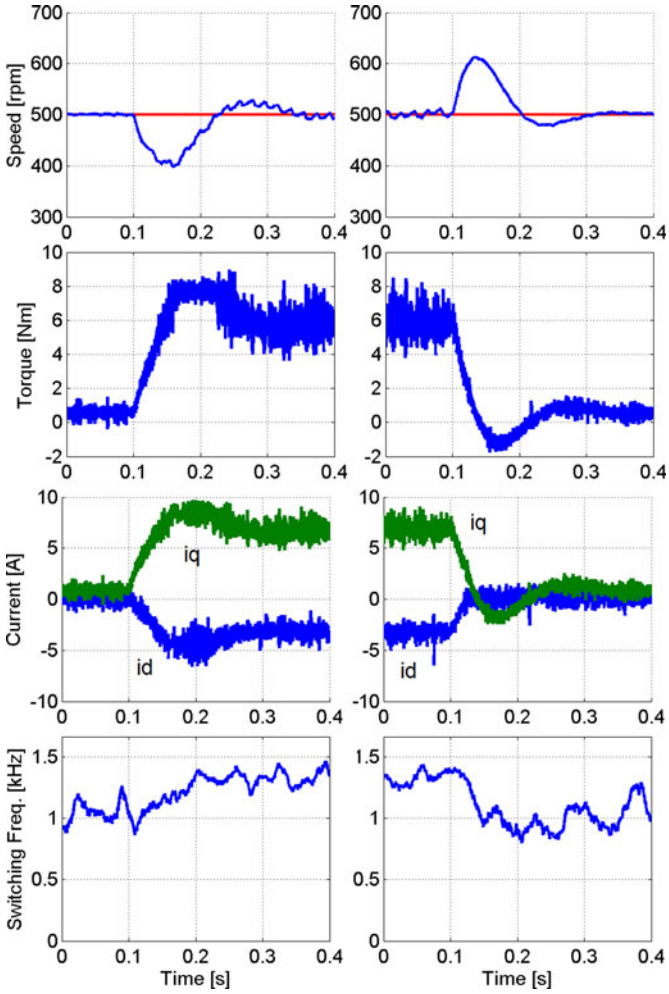

Fig. 9. Experimental result: load torque step; from top: reference and measured speed, electrical torque, *dq* currents, and switching frequency.

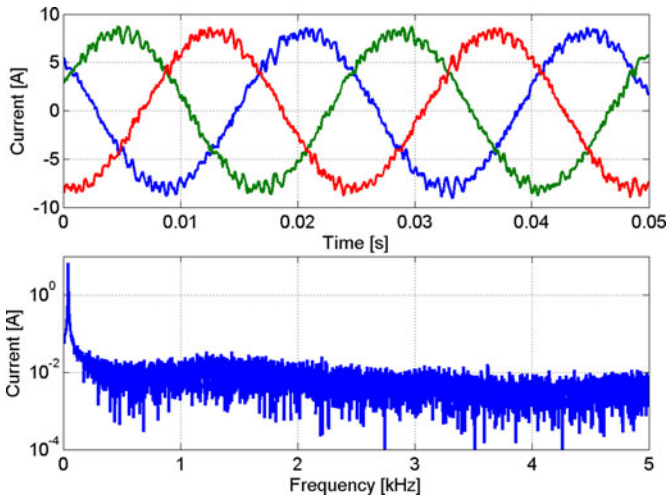

Fig. 10. Simulation result: current waveform and spectrum; THD = 5.9%; average switching frequency about f_{sw} = 1.25 kHz.

The spectra shows previously the fundamental frequency and distributed noise with low magnitude. This noise is a consequence of the stochastic choice of plant inputs. Some low

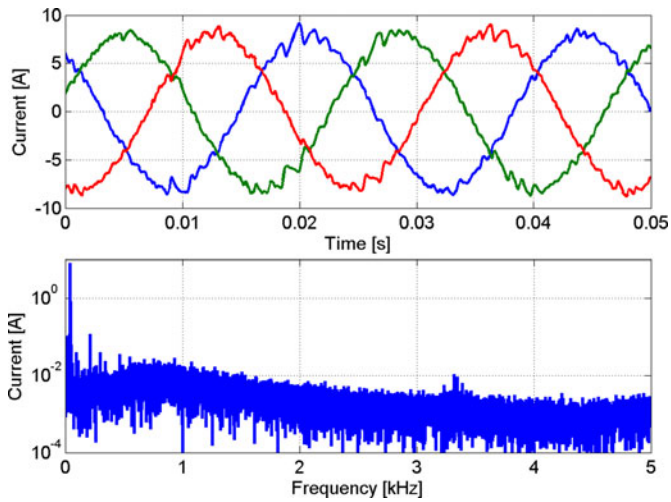

Fig. 11. Experimental result: current waveform and spectrum; THD = 4.7%; average switching frequency about $f_{\mathrm{sw}} = 1.25$ kHz.

frequency odd harmonics which are not the multiples of three are observed in the experimental result. However, the magnitudes of both noise and harmonics can be accepted considering the average switching frequency. For both systems, the THD has been computed. It is THD = 5.9% in simulation and THD = 4.7% in experimentation. If a higher switching frequency is acceptable, the THD can be reduced using a smaller sampling period.

In the experimental spectrum, some harmonics are pointed out at 3.3 kHz. This frequency corresponds to the mechanical resonance frequency of the test bench. They are not observed in simulation since the plant has been modeled with a single-mass-equivalent system.

V. Conclusion

In this research, MP-DSC has been developed and implemented. The concept is based on the MPC approach with finite control set. The possible plant inputs are applied to an online plant model and their effects are predicted, which can be repeated until the prediction horizon is reached. The results are fed to a decision or cost function, which is used to decide the plant input, i.e., the converter switching state for the next sampling period.

MP-DSC has been evaluated by simulation and the results confirm the dynamic advantages of the concept. The overall control behavior has been evaluated with reference and disturbance steps. MP-DSC shows promising result with respect to both. Moreover, MTPA tracking is obtained and leads to high efficiency. The major plant disturbance, i.e., the load torque, would lead to a prediction and, thus, to steady-state speed offsets. A compensator is proposed and its effectiveness is shown. The MP-DSC dynamics has been quantified with the approximative *bandwidth–rise time* relation assuming a Gaussian response system. The bandwidth without saturation active is in the order of 100 Hz (compared with the switching frequency which is in the order of 1 kHz). However, significant reference or disturbance steps will usually push the torque into limitation which reduces the raise time according to the limit. Furthermore, the steady-state current quality is discussed. The spectra previously show noise, which is obtained due to the stochastic selection of the plant inputs. Some low-order harmonics are pointed out, but the current, i.e., torque quality, can be generally accepted considering the switching frequency.

References

[1] P. Cortés, M. P. Kazmierkowski, R. M. Kennel, D. E. Quevedo, and J. Rodríguez, "Predictive control in power electronics and drives," *IEEE Trans. Ind. Electron.*, vol. 55, no. 12, pp. 4312–4324, Dec. 2008.

[2] L. Malesani, P. Mattavelli, and S. Buso, "Robust dead-beat current control for pwm rectifier and active filters," *IEEE Trans. Ind. Appl.*, vol. 35, no. 3, pp. 613–620, May/Jun. 1999.

[3] J. Holtz and S. Stadtfeld, "A predictive controller for the stator current vector of ac machines fed from a switched voltage source," in *Proc. IPEC*, 1983, pp. 1665–1675.

[4] M. Depenbrock, "Direct self-control (DSC) of inverter-fed induction machine," *IEEE Trans. Power Electron.*, vol. 3, no. 4, pp. 420–429, Oct. 1988.

[5] S. V. Emeljanov, *Automatic Control Systems With Variable Structure*, R. Oldenbourg-Verlag: Munich Germany, 1969.

[6] I. Takahashi and T. Noguchi, "A new quick response and high efficiency control strategy of an induction motor," in *Proc. IEEE IAS*, 1985, pp. 1665–1675.

[7] P. Mutschler, "A new speed-control method for induction motors," in *Proc. PCIM*, 1998, pp. 131–136.

[8] L. Jinglin and C. Junshuo, "Predictive control for permanent magnet synchronous machine based on automatic differentiation method," in *Proc. Int Electr. Mach. Syst. Conf.*, 2011, pp. 1–4.

[9] N. Hoffmann, S. Thomsen, and F. W. Fuchs, "Model based predictive speed control of a drive system with torsional loads—a practical approach," in *Proc. 14th Int. Power Electron. Motion Control Conf.*, 2010, pp. T5-149–T5-156.

[10] E. Fuentes, C. Silva, and J. Yuz, "Predictive speed control of a two-mass system driven by a permanent magnet synchronous motor," *IEEE Trans. Ind. Electron.*, vol. 59, no. 7, pp. 2840–2848, 2012.

[11] T. Geyer, "Computationally efficient model predictive direct torque control," *IEEE Trans. Power Electron.*, vol. 26, no. 10, pp. 2804–2816, Oct. 2011.

[12] K.-J. Lee, B.-G. Park, R.-Y. Kim, and D.-S. Hyun, "Robust predictive current controller based on a disturbance estimator in a three-phase grid-connected inverter," *IEEE Trans. Power Electron.*, vol. 27, no. 1, pp. 276–283, Jan. 2012.

[13] C. D. Townsend, T. J. Summers, and R. E. Betz, "Multigoal heuristic model predictive control technique applied to a cascaded h-bridge statcom," *IEEE Trans. Power Electron.*, vol. 27, no. 3, pp. 1191–1200, Mar. 2012.

[14] Z. Shen, X. Chang, W. Wang, X. Tan, N. Yan, and H. Min, "Predictive digital current control of single-inductor multiple-output converters in ccm with low cross regulation," *IEEE Trans. Power Electron.*, vol. 27, no. 4, pp. 1917–1925, Apr. 2012.

[15] M. Preindl, E. Schaltz, and P. Thøgersen, "Switching frequency reduction using model predictive direct current control for high power voltage source inverters," *IEEE Trans. Ind. Electron.*, vol. 58, no. 7, pp. 2826–2835, Jul. 2011.

[16] M. Preindl and E. Schaltz, "Sensorless model predictive direct current control using novel second-order PLL observer for PMSM drive systems," *IEEE Trans. Ind. Electron.*, vol. 58, no. 9, pp. 4087–4095, Sep. 2011.

[17] R. P. Aguilera and D. E. Quevedo, "On stability and performance of finite control set mpc for power converters," in *Proc. Workshop Predictive Control Electr. Drives Power Electron.*, 2011, pp. 55–62.

[18] M. Preindl and E. Schaltz, "Load torque compensator for model predictive direct current control in high power PMSM drive systems," in *Proc. IEEE Int. Symp. Ind. Electron.*, 2010, pp. 1347–1352.

[19] D. Luenberger, "Observing the state of a linear system," *IEEE Trans. Mil. Electron.*, vol. 8, no. 2, pp. 74–80, Apr. 1964.

[20] S. Bolognani, R. Petrella, A. Prearo, and L. Sgarbossa, "Automatic tracking of mtpa trajectory in ipm motor drives based on ac current injection," in *Proc. IEEE Energy Convers. Congr. Expo.*, 2009, pp. 2340–2346.

[21] M. Preindl and S. Bolognani, "Model predictive direct torque control with finite control set for PMSM drive systems," *IEEE Trans. Ind. Inf.*, to be published.

[22] M. Preindl and S. Bolognani, "Model predictive direct torque control with finite control set for PMSM drive systems: Field weakening operation," *IEEE Trans. Ind. Inf.*, to be published.
[23] W. S. Levine, *The Control Handbook*. Boca Raton: FL: CRC Press, 1996.

Matthias Preindl was born in Brixen, Italy, in 1986. He received the B.Sc. degree (*summa cum laude*) from the University of Padova, Padova, Italy, in 2008, and the M.Sc. from ETH Züurich, Switzerland, in 2010, both in electrical engineering. He is currently working toward the Ph.D. degree in energy engineering at the University of Padova,.

He has been Visiting Student at Aalborg University, Denmark, where he wrote his diploma thesis. From 2010 to 2012, he was with Leitwind AG, Italy, where he was an R&D engineer. Before that, he worked for Energy.dis GmbH, Italy, and the Italian National Research Council (CNR-RFX). He is currently a Visiting Scholar at the University of California, Berkeley. His research interests include control and design of power electronic systems with applications in drive systems, renewable energy generation, and vehicular systems.

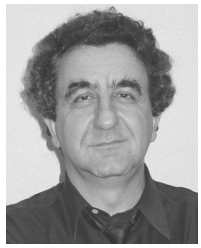

Silverio Bolognani (M'76) received the Laurea degree in electrical engineering from the University of Padova, Padova, Italy, in 1976.

In 1976, he joined the Department of Electrical Engineering, University of Padova, where he is currently a Full Professor of electrical converters, machines, and drives. He then started the Electrical Drives Laboratory, where a variety of research works on brushless and induction motor drives is carried out in the frame of the European and the national research projects. He is the author of more than 200 papers on electrical machines and drives and is the holder of three patents.

Prof. Bolognani is currently the Chairman of the IEEE North Italy IEEE Industry Applications/Industrial Electronics/Power Electronics Societies Joint Chapter. He has been serving international conferences as a member of the Steering or Technical Committees, as well as an Invited Speaker.